Electron Impact Excitation of Autoionizing Levels of Kr and Xe between the $^2P_{3/2}$ and $^2P_{1/2}$ ionic Limits

Lance R. LeClair[1] and Sandor Trajmar

Jet Propulsion Laboratory, California Institute of Technology

Pasadena, CA, 91109, USA

[1]National Research Council Resident Research Associate

P.A.C.S. # 34.80.Gs

E-mail Addresses:

L. LeClair: LANCER@SCN1.JPL.NASA.GOV

S. Trajmar: SANDOR@SCN1.JPL.NASA.GOV

Abstract

We have observed electrons ejected from autoionizing levels which lie between the $^2P_{3/2}$ and $^2P_{1/2}$ ionic limits for Kr and Xe. Kinetic energy spectra of the ejected electrons were obtained following electron impact excitation of the target gases by using time-of-flight spectroscopy in a crossed beam experiment. Spectral features which correspond to electrons ejected from both odd and even parity autoionizing levels have been identified. Some of the features have kinetic energies of just over 0.1 eV and have been resolved for the first time in an electron impact experiment. The most intense features at low electron impact energies come from optically forbiden np′ and nd′ terms. It was possible to estimate the integral cross section for autoionization by comparing the intensity of the elastically scattered electrons with the intensity of the autoionizing features. For Xe, autoionization from the levels which lie. between the ionic limits appears to account for about **67%** and **7.6%** of the electron impact ionization cross section at impact energies of 14 and 24 eV, respectively; while for Kr, the fractions are 20% and 2.7% at 16 and 26 eV.

1. Introduction

Autoionization is a fascinating phenomenon which has attracted considerable experimental and theoretical interest. The autoionizing levels of heavy rare gases which lie between the $^2P_{3/2}$ and $^2P_{1/2}$ ionic limits (hereafter referred to as the low Al levels) have been the subject of many photon impact studies in recent years. These efforts have utilized single photon excitation from the ground state (e.g. Maeda et al. 1993) and multiphoton excitation from the ground state or metastable levels (e.g. Wang and Knight, 1986; Klar et al., 1992.; Koeckhoven et al. 1994, 1995) in order to obtain energies, lineshapes, lifetimes, quantum defects, and photoabsorption cross sections for many of the low Al levels. The use of multiphoton techniques has enabled many of the otherwise optically forbidden low Al levels to be reached.

Even though electron impact excitation of the low Al levels can be a significant ionization channel, such studies have attracted much less attention, possibly because of experimental difficulties. Electron impact excitation of an Al level from the ground state proceeds as follows,

$$e(E_o) + X \rightarrow e(E_r) + X^*(\Delta E)$$

$$X^*(\Delta E) \rightarrow X^+ + e(E_{ej}) ,$$

where $E_o = E_r + \Delta E$, E_o is the kinetic energy of the incident electron, E_r is the residual energy of the scattered electron, and ΔE is the excitation energy of the autoionizing level (that is, the energy lost by the incident electron). Note that dipole selections rules can be thrown out since electron exchange can take place if E_o is low enough. Since X^* lies in the ionization continuum, it can autoionize by ejecting a second electron with energy $E_{ej} = \Delta E - E_i$, where E_i is the ionization energy of X. One additional complication arises from the fact that autoionizing levels are very short lived (from fs to ps lifetimes). If E_r is very small (several meV) the scattered electron may still be in the neighborhood of the excited target when the second electron is ejected (depending on the lifetime) and a post-collision interaction (PCI) between the two electrons will

occur.

Electron impact excitation of autoionizing levels can be studied by detecting the product ion, the scattered electron, or the ejected electron; either separately, or in coincidence. The only previous electron impact studies of the low Al levels of rare gases have. been those of Marmet and Proulx (1 990), and Hammond et al. (1 988). Marmet and Proulx observed the low Al levels as small perturbations to the total Xe^+ production curve, measured as a function E_o. Hammond et al. have observed the low Al levels by ut i] i zing threshold elect ron energy loss spectroscopy (EELS). In their case, only electrons with $E_r < 2,()$ meV were? collected as a function of E_o. The ensuing results were particularly useful for a study of PCI effects (Read and Hammond, 1988). There arc other electron impact studies of Al levels in rare gases (e.g. scc Comer, 1992; Baxter et al., 1982), but those were concerned with levels which produced ejected electrons with energies greater than several eV. This was probably because electrons with such kinetic energies arc easi I y anal yzed with convent ional elect ron energy spect rometers employing elect rest atic dispersive elements. Electrons with kinetic energies of a fcw tenths of an eV arc difficult to observe wit h a convent ional elect rost at ic spect rometers because low energ y elect rons are more susceptible to the aberrations and surface conditions of the lenses which arc employed to collect the electrons and guide them through the dispersive. elements of the spectrometer.

Recentl y, wc have construct ed a time-of- flight (TOF) electron spectrometer which is free of focusing and energy-dispcrsil]g electric and magnetic fields. This spectrometer was utilized to measure ratios between inelastically and elastically scattered electrons (from gaseous targets) which arc free from the instrumental c! ffects encountered with conventional electrostatic spectrometers. These ratios, in turn, can ser vc as secondary standards for normalizing inelastic di fferent ial cross sections obt ained from measurements made with conventional elect rostat ic spect rometers (LeClair and Trajmar, 1996). During our work with rare gases, we noticed the

appearance of sharp structures at very long flight times which were due to electrons ejected from the low Al levels. We studied the ejected electron spectra obtained from Kr and Xc and the results of this short investigation are presented below.

2. Apparatus and method.

A brief description of the apparatus will be given only since a detailed description has already been published (1 .eClair et al., 1996). Essentially, the apparatus consisted of a mutually orthogonal electron beam, gas beam, and drift tube. These items were placed in a magnetically shielded (< 2 mgauss) vacuum chamber and baked at 1 50°C to maintain clean surfaces.

We used a simple electron gun which is capable of producing a highly collimated electron beam of up to 220 nA in the d.c. mode, from 2 to several hundred CV impact energies. When operated in the pulsed mode, the gun typically produced gaussian pulses with widths of several nanoseconds, depending on E_o. We calibrated E_o by observing the threshold of metastable product ion for each target gas with a neutral metastable detector. There were no energy dispersing elements in the gun, so the energy width of the electron beam was about 0.6 CV (FWHM), which is typical of thermionic sources.

The drift tube was constructed out of sheet molybdenum and had two apertures to define a view cone with an apex of 6". The end of the drift tube was terminated with a grid, followed by a post-acceleration voltage of 450 V onto a stack of 40 mm diameter multi-channel plate electron multipliers. The field free drift distance for scattered electrons was 21.6 cm, giving an electron time-of-flight, t (ns), of

$$t = 364/\sqrt{E}, \qquad (1)$$

where E is the kinetic energy of the electrons in eV. The kinetic energy resolution for

ejected electrons is predominantly given by

$$\delta E = 2E\delta t/t \qquad (2)$$

where δt represents the temporal width of the incident electron pulse. Thus the energy resolution improves for lower kinetic energies.

TOF spectra were acquired by using a time-to-amplitude convertor ('l"AC) in conjunction with a pulse height analyzer which operated under the control of a persona] computer. The time scale was calibrated with a high precision digital delay generator. The pulse rate of the electron gun was 100 KHz.

To aid interpretation Of features in the TOF spectra, it is convenient to convert them to kinetic energy spectra by a change of variable. That is, if $F(t)$ represents a TOF spectrum, then its kinetic energy spectrum, $F(E)$, is given by

$$F(E) - F(t)t^3 \ . \qquad (3)$$

One must exercise caution when interpreting features in the kinetic energy spectrum since the t^3 factor in (3) greatly exaggerates noise at long flight times. We applied Gram's method of smoothing to the spectra to reduce the noise (Hildebrand, 1987). Also, careful attention must be paid to background subtraction before the transform is done. We used the background in our TOF spect rum which occurred past 1800 ns. The count rate during data acquisition was less than 500 cps, so there was no tilting of the background due to TAC pile-up. The accuracy of the kinetic energy scale depends on the linearity of TAC and the location of the t = O mark in our TOF spectra. The linearity was checked with a precision digital delay generator, and amounted to a ±1 ns deviation over 1000 ns. The t = O mark was located with respect to the maximum of the elast ic scattering feat ure present in each TOF spect rum and calculated by using equation (1) and the calibrated electron impact energy. This was accurate to within ±2 ns. Thus the accuracy of the kinetic energy scale for a feature at 540 ns (see

figure 2.) is about ± 4 meV (from equation (2)), and this improves with increasing time-of-flight.

3. Results and discussion.

A TOF spectrum resulting from electron impact on Xc is shown in figure 1. The prominent features due to elastic and inelastic scattering, and the autoionizing features are labelled in the figure, Note that for every ejected electron feature in figure 1, there must be an inelastic feature corresponding to the scattered electron. Such features are not resolved in our TOF spectra because the temporal width for inelastic features depends on the electron pulse width and the energy distribution of the incident electron beam (0.6 eV). However, the temporal width of an ejected electron feature is determined by the duration of the incident electron pulse and the natural lifetime of the Al level responsible for that feature. In the case where an Al level has a narrow energy width (but with a lifetime short compared to the incident pulse) then the width of the Al feature in the TOF spectrum is approximately equal to the duration of the incident pulse. By inspection of feature g in figure 4 it was deduced that the incident pulse width was about 10 ns since the lifetime of the associated level (Xc $8s'[^1/_2]1$) is about 250 fs (Wang and Knight, 1986). This gives an instrumental energy width for that feature of about 20 meV (the natural width is about 2.6 meV). We would like to point out that we did find some small features in the TOF spectra caused by reflection of the incident electron pulse off of some of the structures in the vacuum chamber. However, these "echo" features occurred much earlier in time than the autoionization features. Moreover, they changed shape and decreased in flight time with increasing electron impact energy. The autoionization features occurred at the same time-of-flight regardless of impact energy, as long as E_o exceeded a characteristic threshold value.

Singly excited levels of heavy rare gases are characterized best by the *jl* coupling scheme, in which the orbital angular momentum *l* of the excited electron is strongly coupled to the

angular momentum j of the ion core, forming a resultant angular momentum K. K is then weakly coupled to the electron spins, giving total angular momentum J. The core levels are $np^5\ ^2P_{1/2}$ and $^2P'_{3/2}$ (with inverted fine structure), giving $j = {}^1/_2, {}^3/_2$. Notation is $nl[K]J$, with a prime (') *cm 1* implicating $j = {}^1/_2$.

a. Xe

The results from Xe will be discussed first since most of the present work was done on it because of its larger autoionization cross section. Kinetic energy transforms of TOF spectra obtained from Xc for electron impact energies of E_o = 14.0, 24.0, and 300 eV are shown in figs. 2, 3, and 4, respectively. The features due to electrons ejected from autoionizing levels are labelled a through k, in correspondence with fig. 1; and there is feature 1, which appears in figure 4 only. Identification of the levels responsible for features a to l are indicated in table 1. Table 1 lists the some of the superexcited levels of Xc between the ionic limits and their corresponding excitation energies. The ejected electron kinetic energy spectra of figs. 2 and 3 were acquired using an electron beam of 10 nA (the current was measured in the d.c. mode) and each took 48 hours to acquire. It was much quicker to acquire spectra at higher beam CUJ rent (fig. **4** was acquired in 8 hours at **200** nA current), but we found that the positions of the features shifted somewhat to higher kinetic energies (from their spectroscopic values) with increasing electron beam current. We also observed that the shift was not exactly the same for each feature. Wc are unsure of the reason for the shift, but believe that it is a complex interplay of space charge and sulfate conditions in the interaction region which are affected by electron beam current. We studied the current dependent shift only for Xe and only at 14 eV electron impact energy. Time did not permit us to study it at other energies and for Kr.

One obvious observation of figs. 2, 3, and 4 is the change in structure with electron

impact energy. This arises from the well known behavior of elect rcm impact excit at ion cross sections for optically forbidden and optically allowed transitions. Electron impact excitation cross sections for levels accessible by optically forbidden transitions peak rapidly within a few CV of threshold and fall off nearly as rapidly. Features a to e, and h behave this way, being prominent in figs. *2* and 3, but absent from fig. *4*. Conversely, cross sections for optically allowed transitions gradually increase to reach a maximum which may be dozens of eV above threshold, and then fall off, usually more gradually than the rise to the maximum. Examples here arc features f and g which belong to the nd′[$^3/_2$] 1 and ns′[$^1/_2$]1 rydberg series and are optically accessible from the ground level. Features from these two series are the only ones present in fig. 4 (E_o = 300 eV). Note that in fig. 4 the s' series members with n>8 appear as shoulders to the d' series since the resolution gets worse for higher ejected energies, see equation (2). The resemblance between the ejected electron energy spectrum of fig. 4 and photoabsorption spectra of the nd′[$^3/_2$] 1 and ns′[$^1/_2$] 1 series of the heavy rare gases (Maeda et al., 1993) is remarkable, even reproducing the asymmetric Beutler-Fano profile of the nd′[$^3/_2$] 1 levels. This is yet another example of how electron collisions mimic photon collisions at high energies (Inokut i, 197 1).

Features a, b, and c originate, from the 7p' [$^3/_2$]1, the unresolved 7p' [$^1/_2$]1 plus 7p′[$^3/_2$]2, and the 7p′[$^1/_2$]0 autoionizing levels of Xc, respectively. They are very prominent, as are the higher members of np′ series, at low electron impact energies. The excitation energies of these levels have been measured accurately (Grandon and Husson, 1981; Koeckhoven et al., 1995). Feature c may appear to be indiscernible from noise in fig. 2, but it is real; it could be seen more clearly by increasing the electron current. Features a, b, and c did not shift any noticeable amount as a function of current up to 100 nA, but by 200 nA it was about 20 meV. Their positions match the spectroscopic values in the E_o =- 14 eV spectrum (fig. 2) but their positions

are shifted by about 10 to 20 meV below their spectroscopic values at $E_o = 24$ eV (fig. 3). We attribute this to slowly building surface patch fields within the drift tube, since fig. 3 was acquired after fig. 2. Those patch fields probably account for the fairly sharp cut off of electrons with energies below 0.1 eV in the kinetic energy spectra. As surface, patch fields gradually grew worse with time, autoionizing features shifted to lower kinetic energies, and the slowest features would disappear from the spectra,

Features d and e are probably from two of the $6d'[^5/_2]2$, $6d'[^3/_2]2$, and the $6d'[^5/_2]3$ Al levels, with the third being unresolved or absent. We could find no spectroscopic measurements for the excitation energy of these levels. Instead we used the quantum defect for the $nd'[^5/_2]3$, n = 8-40 levels measured by Koeckhoven et al., 1994, and interpolated with the quantum defect for the n = 5 level (Moore, 1957). There was practically no change in the quantum defect from n = S to n = 8, so we estimate our calculated energy is close to within ().01 eV. We calculated the energies of other Al levels in similar fashion, and these have been denoted by an asterix in Table 1. A kinetic energy shift of up to 40 meV at 220 nA was observed for these features.

Feature f, as we mentioned above, arises from the $6d'\ [^3/_2)1$ level, which is optically accessible from the ground state. Feature f is mostly absent from fig. 2, apparent in fig. 3, and very strong in fig. 4.; typical for electron impact excitation of levels which are accessible by optically allowed transitions. The enormous width of feature f (relative to the others) comes from its extremely short lifetime, about 27 fs (Maeda et al., 1993). The maximum of our feature is slightly higher than the measured spectroscopic value (Maeda et al., 1993), and this may be due to PCI since the lifetime is so short. If an electron is ejected while the scattered electron is nearby, the ejected electron acquires extra kinetic energy since it is no longer escaping an ion, but a dipole.

There are six different unresolved levels which could contribute to feature g (see table 1).

The optically allowed 8s'[$^1/_2$]1 level probably contributes the most to the intensity at E_o = 24 eV and above (figs. 3 and 4) and whi le the optically forbidden 8s' [$^1/_2$]0 and 4f' levels probably dominate at E_o = 14 eV (fig. 2). By plotting the energy shift of feature g as a function of current, it was observed that the shift had practically disappeared (to within a few mcV) when extrapolating to zero current. The shift was not a linear function of current, but appeared to be reaching some asymptote with increasing current,

Feature h is made up of 8p' and 7d' levels which cannot be reached by an optically allowed transit ion from the ground state. 1 'eat ure i is from the 7d' [$^3/_2$]1 level, and appears to be shifted by 10 meV above its spectroscopic energy, but it is not clearly resolved. Feature j is due to overlapping 9s' and 5f' levels, feature k arises from 8d' and 9p' levels, and the last assigned feature is 1 (fig,. 4 only), from the 9d'[$^3/_2$] 1 level. Higher up the energy scale the remaining feat ures overlap, forming a smooth continuum, until the abrupt drop at the $^2P_{1/2}$ ionic limit.

We have searched the literature and found only one other example of an ejected electron energy spectrum for Xc for the low Al levels. in that work (Penent et al., 1990), Xe atoms were bombarded by H“ ions at 5 **KeV. A 127°** cylindrical analyzer was used to obtain an ejected elect ron spectrum which closely resmbles ours, except the feat ures which lie below ().4 eV do not appear in their spectra, It may be possible that PCI with H⁻ ions has something to do with this, but it is more likely that it was caused by an instrumental effect in their energy analyzer since, as stated earlier, it becomes increasingly difficult to collect, focus, and analyze electrons as their kinetic energy decreases. This illustrates one advantage of using TOF electron spectroscopy over conventional elect rest at ic EEL,S.

Another advantage of TOF spectroscopy is that a direct comparison of the intensit y of (wo different features in a TOF spectrum can be made without factoring in the instrumental collection efficiency, as is done with conventional electrostatic electron energy analyzers. Thus, it is

possible to calculate the electron scattering differential cross section (DCS) for one feature, by means of comparison with another feature. for which the DCS is known. This has been discussed our previous paper (1 .eClair and Trajmar, 1996) and can be briefly described as follows. First, the intensity of the elastic feature is used since elastic DCS's are well established, and the elastic feature in TOF spectra is usually well separated from other features. The scattering intensity associated with the elastic feature (I_{el}) is related to the elastic DCS by the following proportionality:

$$I_{el}(E_o,0) \alpha \int j(x,y,z) n(x,y,z)\, DCS_{el}(E_o,0) \Delta\Omega(x,y,z)\, dV \cdot , \quad (4)$$

where j is the current density; n is the number density of gas molecules which make up the target; DCS_{el} is the elastic differential cross section at E_o and 0; A Ω is the view cone into whit.1~ the scattered electrons are collected; and dV is the volume element located at position (x, y, z). The scattering intensity associated with an inelastic feature (I_{inel}) is related to the inelastic DCS by the same proportionality, equation (4), except DCS_{el} is replaced by DCS_{inel}. By taking a ratio of the. two proportionalities one obtains $DCS_{inel} = DCS_{el}\, I_{inel}/I_{el}$ for a given E_o and o.

For electron impact excitation of autoionizing levels this method cannot be applied since, as stated earlier, the scattered electrons causing excitation of individual autoionizing levels cannot be resolved in the present TOF spectra. Thus, the DCS for scattering from those levels cannot be determined. However, it is possible to obtain a reasonable estimate of the integral cross sect ion for elect ron impact excitation of an autoionizing level by a comparison bet ween the intensity of features due to elastically scattered electrons and ejected electrons. This estimate requires two assumpt ions. First, *it is assumed that the ejected electrons are emitted isotropically.* We have no means to test this assumption with the present apparatus. It certainly cannot hold

if PCI takes place. Secondly, the autoionizing features in the kinetic energy spectra are not peaks but Beutler-Fano profiles superposed on a background of elect rons associated with the $^2P_{3/2}$ continuum. Beutler-Fano profiles typically have a portion which extends above the continuum and one which extends below. *It is assumed that the negative going portion of the Beutler-Fano profile is very small* since wc see no evidence of it in the kinetic energy spectra, Thus the features can be treated as peaks on a background and their intensities can be easily determined. The intensity of an ejected electron feature. (I_{AI}) is then related by the following proportionality:

$$I_{AI}(E_o) \alpha \int j(x,y,z) n(x,y,z) \sigma_{AI}(E_o) \Delta\Omega(x,y,z)\, dV/(4\pi)^{*}, \quad (5)$$

where σ_{AI} is the integral cross section for electron impact excitation of an autoionizing level. Dividing **(5)** by **(4) we** obtain

$$\sigma_{AI} = 4\pi R DCS_{el}(E_o,0) \quad (6)$$

where $R = I_{AI}/I_{el}$, the ratio of the intensities obtained from the TOF spectra.

Equation (6) was applied to most features in figures 2 and 3 and the results for R and o appear in Table 1. The values for $DCS_{el}(0=90^{\circ})$ for Xe at 14 and 24 eV were obtained by interpolat ion of the experimental data of Register et al, (1986) (46 and 19 x 10^{-18} cm^2/st er respectively, ± 30%). The errors in calculating R are estimated to be between 25 and 75% because of the overlap between features which required unfolding, and the uncertainty in the background. For the background, wc fitted two exponentials to trace out the minima which appear bet ween the feat ures a to k in the TOF spect ra. An example is shown in figure 1. By subtract ing this reasonable estimate for the backgr ound, we were also able to obt ain the total autoionization intensity and calculate the integral cross sections for autoionization by all levels between the ionic limits for impact energies of 14 and 24 eV. These arc plotted in figure 5 along with the integral cross section for electron impact ionization of Xe as measured by Krishnakumar

and Srivastava (1988). At 14 cV, electron impact ionization by means of autoionization accounts for about 2/3 of the ionization cross section, and this drops to about 7.5% at 24 eV.

Note that in equation (6) wc are comparing the intensities which come from low energy elect tons (<1 cV) with those of higher energy (by more than a factor of 10), We cannot say for certain that all of the low energy electrons are being collected as efficiently as the higher energy clcctr-ens, owing to patch fields, etc., and so our cross sections must be considered an est i mat e, and possibl y a lower bound estimate.

h Kr

Kinetic energy spectra of electrons ejected from the low autoionizing levels of Kr are shown in figures 6 and 7 for E_o = 16 and 26 cV, respectively. They were both obtained using 10 nA of electron current. Due to a lack of time and a change of research interests we were not able to obtain spectra at higher current and electron impact energy. The features arc labelled a to 1 and identified in Table 2. The energies which are listed in 'liable 2 came from spectroscopic measurements by Delsart and Keller (1 983), Wada et al. (1987), Klar et al. (1992), Maeda at el. (1993), and Koeckhoven et al. (1994 and 1995). Wada et al. (1987) obtained measurements for the 7d' levels only. Since there arc no measurements of the energies of the remaining members of the nd' series, those energies were calculated from the quantum defects for the 7d' levels, except for the optically allowed nd' $[^3/_2]1$ levels for which accurat e measurements exist (Maeda et al., 1993).

The Kr data was acquired following our work with Xc. Surface patch fields had increased such that the kinetic energy spectra from Kr had to be shifted by about 25 meV in order to identify the features. This was determined by shifting the kinet ic energy spectrum taken at E_o = 26 eV so that features a and e matched the spectroscopic energies of the 8s'$[^1/_2]1$ and 7d' $[^3/_2]1$

levels, respectively. Both features a and c are absent from the spectrum taken at 16 eV, hence they must be associated with levels which arise from optically allowed transitions. The 25 meV shift resulted in a good match between the remaining features and their spectroscopically determined energies,

As with the kinetic energy spectrum obtained from Xe, there is a sharp drop in intensity in figures 6 and 7 below 0.1 eV which is attributed to patch fields in the drift tube. This leads to a greatly diminished intensity for feature a (compared to Xc). Feature a appears to be indiscernible from the noise which surrounds it, but it dots appear in the TOF spectrum as a small bump at 1340 ns. The width of feature a is approximately 5 mcV. To the left of feature a one can see what appears to be structure from the 6d' terms, but we could not discern anything from the background in the TOF spectra in that range (over 1500 ns). Feature b appears to be due to the 5f' terms; some structure can be discerned at 16 eV, but little. else at 26 eV, possibly due to the distortion from the patch fields.

Feature c can probably be associated with the 8p' term, even though it is slightly lower in energy than spectroscopic measurements, since half oft he fine structure. levels of the 8p' term have not yet been measured. Feature d arises from the unresolved 7d' [$^5/_2$]2, 7d' [$^5/_2$]3, ant] 7d' [$^3/_2$]2 terms. As in the case with Xe, both the np' and nd' autoionizing series arc very intense at these impact energies. As stated earlier, feature e arises from the optically allowed 7d'[$^3/_2$]1 level, and feature f from the 9s' and 6f' terms. Features g, h, and i are simply the next higher members of the levels which contributed to features c, d, c, and f. Likewise, feature j is made up of the next higher members of the levels in features g, h, and i, but they arc unresolved, Similar assignments apply to features k and 1.

Compiled in Table 2 are the ratios and calculated integral cross sections associated with some of the features, along with the summed cross sections for all the low AI levels in Kr. The

values for $DCS_{el}(\theta = 90°)$ for Kr at 16 and 26 eV were obtained by interpolation of the experimental data of Danjo (1 988) (40 and 24 x 10^{-18} cm^2/ster respectively, ±20%). The total low AI level cross sections have also been plotted in figure 5 for comparison with the total ionization cross section of Kr by electron impact as measured by Krishnakumar and Srivastava (J 988). The results are similar to those obtained from Xc, except that the fraction of the total ionization cross section clue to autoionization is smaller.

4. conclusion

Kinetic energy spectra of electrons ejected from autoionizing levels of Kr and Xc which lie between the $^2P_{3/2}$ stud $^2P_{1/2}$ ionic limits have been obtained using field-free TOF electron spectroscopy. An attempt was made to obtain the same from Ar, but no features could be resolved. For Kr and Xc it was possible to see distinct features due to AI from particular energy levels; and produce a reasonable estimate of the electron impact excitation integral cross sections for these levels, with certain assumptions. The assumption that the ejected electrons are emitted isotropically could not be checked since tile. drift tube was fixed at 90°, and the angle could not be changed without substantial redesign and construction, We were also not able to test how well the assumption holds for levels with different Al lifetimes, or with respect to the amount of incident electron current. It would be interesting to continue this work, but not on the present apparatus. Firstly, the pulse width of the electron gun would have to be shortened in order to improve the resolution of the autoionization features. Secondly, and more importantly, our vacuum system cannot maintain the necessary cleanliness required for the length of time it would take to c1o a thorough study. Patch fields attenuated features below 0.1 cV. After two weeks of operation this cut off would increase, low kinetic energy Al features would diminish in intensity or disappear, and higher energy features would shift dramatically, indicating contamination of the

surfaces exposed to the electrons. However, for the time being, the presence of sharp features in the kinetic energy spectra with energies of about 0.1 to 0.2 eV represents a benchmark in EELS, and the measurement of Al excitation cross sections appears to be novel as well.

S. Acknowledgements

This work was carried out at the Jet Propulsion Laboratory, California institute of Technology, under contract with the National Aeronautics and Space Administration. The authors wish to thank M. A. Khakoo for loan of equipment and material.' One of us (1,. R. 1.,) is grateful to the NRC for being awarded a Resident Research Associateship. We also like to thank S. M. Koeckhoven and C. A. de Lange for useful informat ion.

References

Baxter J A, Mitchell P and Comer J 1983 *J. Phys. B: At. Mol. Phys. 1 S* 1105

Bounakhla M, Lemoigne J P, Grandin J P, Husson X, Kucal H, and Aymar M 1993 *J. Phys. B: At. Mol. Opt. Phys.* 26345

Comer J 1992 *Aust. J. Phys.* **45** 309

Danjo A 1988 *J. Phys. B: At. Mol. Opt. Phys.* 213759

Delsart C and Keller J-(: 1983 *Phys. Rev.* A 28845

Grandin J-P and Husson X 1981 *J. Phys. B: At. Mol. Phys.* **14** 433

Hammond P, Read F H and King G C1988 *J. Phys. B: At. Mol. Opt. Phys.* 2.1 3123

1 Hildebrand F B 1987 *Introduction to Numerical Analysis,* chapter 7, Dover, New York

Inokuti M 1971 Rev. Mod. *Phys.* **43** 297

Krishnakumar E and Srivastava S K 1988 *J. Phys. B: At. Mol. Opt. Phys.* **21** 1055

Koeckhoven S M. Buma W J and de Lange C A 1994 *Phys. Rev.* A 493322

Koeckhoven S M, Buma W J and de Lange C A 1995 *Phys. Rev.* A **51** 1097

Klar D, Harth K, Ganz J, Kraft "I', Ruf M-W, Hotop H, Tsemekhman V, Tsemekhman K and Amusia M Ya 19922. *Phys. D - At. Mel, Clusters* **23** 101

LeClair 1. R, Trajmar S, Khakoo M and Nickel J 1996 *Rev. Sci. Instrum.* 67 1753

1 eClair 1. R and Trajmar S 1996 *submitted to J. Phys. B: At. Mol. Opt. Phys.*

Maeda K, Ueda K and Ito K 1993 *J. Phys. B: At. Mol. Opt. Phys.* 261541

Marmet P and Proulx M 1990 *J. Phys. B: At. Mol. Opt. Phys.* **23** 549

Moore C E 1957 *Atomic Energy Levels,* NSRDS-NBS Publication 35, vol. 3, USA

Penent F, Grouard J P, Montmagnon J L and Hall R] 1 990
J. Phys. B: At. Mol. Opt. Phys. **23** 1449

Read F H and Hammond P 1988 *J. Phys. B: At. Mol. Opt. Phys.* **21** *4225*

Register **D** F, Vušković 1. and Trajmar S 1986 *J. Phys. B: At. Mol. Opt. Phys.* 191685

Wada A, Adachi Y and Hirose C 1987 *J. Chin. Phys.* 865904

Wang 1, and Knight R D 1986 *Phys. Rev.* A **34** 3902

Figure Captions

Fig. Time-of-flight spectrum obtained from Xe at E_o = 24 eV, θ = 90°. The elastic and inelastic scattering features arc below 250 ns. Above 250 ns a magnification factor of 2S has been applied. The features which arc clue to electrons ejected from autoionizing levels of Xc arc labelled a to k, The solid line above 250 ns represents a double exponent ial fit to the background caused by electrons ejected from t he cont inuum above the $^2P_{3/2}$ ionic state of Xe^+ (see text for details). The positions of electrons ejected at both ionic limits are shown,

Fig. 2 Kinetic energy spectrum of electrons ejected from Xe for E_o = 14 eV. The energies of the s', p', cl', and f' autoionizing series and their fine structure components are shown for several principle quantum numbers. The exact values of these energies arc listed in Table 1. The $^2P_{1/2}$ series limit is also shown. The features have been labelled a to k, and correspond to the features with the same labels in figure 1. "

Fig. 3 Same as in fig. *2*, but for E_o = 24 eV.

Fig. 4 Same as in figure 2, but E_o = 300 eV and only the optically allowed levels are shown. This spectra was taken using a high electron beam current of 220 nA, and consequently was shifted by about 100 meV. The kinetic energy scale has been adjusted so that the $8s'[^1/_2]1$ feature appears where it should be, at E_{ej} = 0.445 eV, but there remains a slight miss-match between the features and their spectroscopic energies further to the right (see text for details).

Fig. 5 The total integral cross section for electron impact ionization of Kr and Xe (solid lines), interpolated from the data of Krishnakumar and Srivastava (1988). Also shown are the integral cross sections for autoionization by all levels between the $^2P_{3/2}$ and $^2P_{1/2}$ ionic limits of Kr (x) and Xe (+) as determined from the TOF spectra.

Fig. 6 Same as in figure 2, but for Kr at E_o =16 eV. The letters assigned to the features from Kr arc not related to the letters assigned to the features from XC.

Fig. 7 Same as in figure 6, but E_o = 26 eV.

Table J. Partial list of Xc autoionizing levels which lie between the $^2P_{3/2}$ and $^2P_{1/2}$ ionic limits and their spectroscopic energies (first column). Also shown are the ejected electron kinetic energies, the features they correspond to in fig. 3, the energies of those features measured by TOF, the intensity ratio of those features with respect to elastic scattering, and their integral cross sections at E_o = 14 and 24 eV. The ionization potentials used for $Xe^+[^2P_{3/2}]$ and $Xe^+[^2P_{1/2}]$ were 12.130 eV (Grandin and Husson, 1981) and 13.436 eV, respectively (Wang and Knight, 1986). The spectroscopic energies for the table came from the aforementioned references, Maeda et al. (1993), and Koeckhoeven et al, (1994 and 1995). Note that the spectroscopic energies were given in units of cm^{-1} with much more precision than required for this work. They were converted to eV using 1 eV = 8065.541 cm^{-1}, and rounded to five significant figures. The energies denoted by an asterix were obtained by interpolating quantum defects (see text). The J values in parenthesis indicate that no measurement is available for that level.

	Level	Ejected Energy	TOF Feature	TOF Energy	*R* (%)		σ (x 10-18 cm²)	
E (eV)	nℓ'[K]J	E_{ej} (eV)		E_{ej} (eV)	14 eV	24 eV	14 eV	24 a
12.257	7p'[3/2]1	0.127	a	0.110	0.34	.49	2.0	1.2
12.281	7p'[1/2]1	0.151	b	0.150	0.54	1,04	3.1	2.5
12.283	7]) '[3/212	0.153						
12.304	7p'[1/2]0	0.174	c	0.170	0.20	0.61	1,2	1.5
12,342'	6d'[5/2]2	0.212	d,e	0.210	0.68	1.14	4 . 0	2.7
12.355'	6d'[3/2]2	0.225						
12.369*	6d'[5/2]3	0.2.39		0.?.45				
12.431	6d'[3/2]1	0.301	f	0.330		2.00	-	4.8
12.570*	8s'[1/2]0	0.440	g	0.450	0.20	***0.23***	***1.2***	.52
12.575	4f'[7/2]3, 4	0.445						
12.575	4f'[5/2]3	0.445						
12.576	4f '[5/2]2	0.446						
12.576	8s'[1/2]]	0.446						

Table 1. continued

	Level	Ejected Ion: Energy	Feature	TOF Energy	R (%)		σ (x 10^{-18} cm²)	
E (eV)	nℓ'[K]J	$E_{ej.}$ (eV)		$E_{ej.}$ (eV)	14 eV	24 eV	14 eV	24eV
12.736	8]) '[3/2]1	0.606						
12.748	*8p' ['/2] 1*	0.618						
12."149	8p'[3/2]2	0.619						
*12.758**	8p'[1/2]0	0.628	h	0.640	0.29	0.64	1.7	1.5
12."772'	7d'[5/2]2	0.642						
*12.778**	7d'[3/2]2	0.648						
12.785*	7d'[5/2]3	0.655						
12.813	7d' [3/2]1	0.683	i	0,710		0.24	-	0.58
12.885	**9s' ['/2]0**	0.755						
12.886	5f'[7/2]3, 4	0.756	j	0.760	0.071	0.33	0.41	0.80
12.886	5f'[5/2]2, 3	0.756						
12.888	9s'['/2]1	0.769						
12.980	9p'[3/2](1), 2	**0.850**						
12.985	9p'[1/2]0, (1)	**0.855**						
12.991	8d' [5/2]2	**0.861**						
12.993	8d'[3/2]2	**0.863**	k	0.880	0.13	0.54	0.74	1.3
12.998	8d'[5/2]3	**0.868**						
13.013	8d'[3/2]1	**0.883**						
13.054	6f' [7/2] 3, 4	**0.924**						
13.054	6f'[5/2]2, 3	**0.924**						
13.055	10s'[3/2]10	**0.925**						
13.056	10s'[3/2]1	0.926						
13.111	10p'[3/2](11), 2	**0.981**						
13.114	10p'[1/2]0, (1)	0.984						
13.117*	9d'[5/2]2	0.987						
13.119	9d'[3/2]1	0.989						

Table 1. continued

E (eV)	Level nl'[K]J	Ejected Energy E_{ej} (eV)	TOF Feature	TOF Energy E_{ej} (eV)	R (%) 14 eV	R (%) 24 eV	(1 (x 10^{-18} cm^2) 14 eV	(1 (x 10^{-18} cm^2) 24eV
13.121	9d'[$^5/_2$]3	*0.991*						
13.130	9d'[$^3/_2$]1	1.000	1					
13.156	7f'[$^7/_2$]3, 4	1.026						
13.156	7f'[$^5/_2$]2, 3	1.026						
13.157	11s'[$'/_2$]0, 1	1.029						
13.193	11p'[$^3/_2$](1), 2	1.063						
13.195	11p'[$^1/_2$]0, (1)	1.065						
13.196	10d'[$^5/_2$]2	1.066						
13.197	10d'[$^3/_2$]2	***1,067***						
13.199	10d'[$^5/_2$]3	1.069						
13.205	10d'[$^3/_2$]1	1.075						
13.222	8f'[$^7/_2$]3, 4	1.092						
13,222	8f'[$^5/_2$]2, 3	1.092						
13.223	12s'[$'/_2$]0, 1	1.093						
13.436	Xe^+ $^2P_{1/2}$	1.306						
			Total		2.91	9.44	19	23

Table 2. Same as table 1, but for Kr, with E_o = 16 and 26 eV. The ionization potentials used for $Kr^+ [^2P_{3/2}]$ and $Kr^+ [^2P_{1/2}]$ were 14.000 eV and 14.665 eV, respectively (Bounakhla et al, 1993). The spectroscopic energies for the first column were obtained from the measurements of Delsart and Keller (1983), Wada et al. (1987), Klar et al. (1992), Maeda et al. (1993), and Koeckhoeven et al. (1994 and 1995).

E (eV)	12VC1 $n\ell'[K]J$	Ejected Energy E_{ej} (eV)	TOF Feature	TOF Energy E_{ej} (eV)	R (%) 16 eV	R (%) 26 eV	σ (x 10^{-18} cm²) 16 eV	σ (x 10^{-18} cm²) 26 eV
*14.009**	6d '[5/2]2	0.009	-					
14.032*	6d'[3/2]2	0.032	-					
*14.044**	6d'[5/2]3	0.044	-					
14.0'/0	6d'[3/2]1	0.070	-					
15.097	8s'[1/2]0	0.097	a	0.100				
14.099	8s'[1/2]1	0.099						
14.118	5f'[7/2]4, (3)	0.118	b	0.130				
14.119	5f'[5/2]2, (3)	0.119						
14.196	8p'[3/2]2, (1)	0.196	c	0.190	0.075	0.11	0.38	***0.34***
14.204	8p'[1/2]0, (1)	0.204						
14.2.24	7d'[5/2]2	0.224						
14.237	7d'[3/2]2	0.237	d	0.240	0.090	0.10	0.45	0.31
14.244	7d'[5/2]3	0.244						
14.258	7d'[3/2]1	0.258	e			0.051	-	0.15
14.274	9S'[1/2]0	0.274						
14.275	9s'['/2]1	0.275	f	0.275	0.074	0.10	0.38	0.31
14.287	6f'[7/2]4, (3)	0.286						
14.287	6f'[5/2]2, (3)	0.287						
14.332	9p'[3/2]2, (1)	0.332	g	0.335	0.063	0.086	0.32	0.26
14.338	9p'[1/2]0, (1)	0.338						

Table 2. continued

E (eV)	14VCI $n\ell'[K]J$	Ejected Energy E_{ej} (eV)	TOF Feature	TOF Energy E_{ej} (eV)	R (%) 16 eV	R (%) 26 eV	σ (x 10"8 cm²) 16 eV	σ (x 10"8 cm²) 26 eV
14.349'	8d'[5/2]2	0.349						
14.357*	8d'[3/2]2	0.357	h	*0.360*	0.033	0.079	0.17	0.24
14.360*	8d'[5/2]3	0.360						
14.369	8d'[3/2]1	0.369						
14.380	10s'[1/2]0, 1	0.380						
14.387	7f'[7/2]4, (3)	0.387	i	0.'.385	0.042	0.066	'0.21	0.20
14.387	7f' [5/2]2, (3)	0.387						
14.417	10p'[3/2]2, (1)	0.417						
14.420	10p'[1/2]0, (1)	0,420						
*14.427**	9d'[5/2]2	0.427						
14.432*	9d'[3/2]2	0.432						
*14.435**	9d'[5/2]3	0.435	j	0.440	-	0$_{s}$12	-	0.35
14.440	9d'[3/2] 1	0.440						
14.448	1 1s'[1/2]0, 1	0.448						
14.453	8f'[7/2]4, (3)	0.453						
14.453	8f'[5/2]2, (3)	0.453						
14.473	1 1p'[3/2](1), 2	0.473						
14.475	1 1p'[1/2]0, (1)	0.475						
14.480*	10d'[5/2]2	0.480						
*14.483**	10d'[3/2]2	0.483						
*14.485**	10d'[5/2]3	0.485						
14.488	10d'[3/2] 1, (2)	0.488	k	0.490				
14.494	12s'[1/2]0, 1	0.494						
14.498	9f'[7/2]4, (3)	0.498						
14.498	9f'[5/2]2, (3)	0.498						
14.512	12p'[3/2](1), 2	0.512						
14.513	12p'[]/210, (1)	0.513						

Table 2. continued

E (eV)	Level $n\ell'[K]J$	Ejected Energy E_{ej} (eV)	TOF Feature	TOF Energy E_{ej} (eV)	R (%) 16 eV	R (%) 26 eV	σ (x 10^{-18} cm^2) 16 eV	σ (x 10^{-18} cm^2) 26 eV
14.516*	$11d'[^5/_2]2$	0.516						
14.519*	$11d'[^3/_2]2$	0.519						
14.520*	$11d'[^5/_2]3$	0.520						
14.523	$11d'[^3/_2]1$	0.523	1	0.540				
14.527	$13s'[^1/_2]0, 1$	0.527						
14.530	$1\,of'\,[^7/_2]4$, (3)	0.530						
14.530	$1\,0f'\,[^5/_2]2$, (3)	0.530						
14.665	$Kr^+\ ^2P_{1/2}$ limit	0.665						
			Total		1.05	*2.02*	*5.3*	6.1

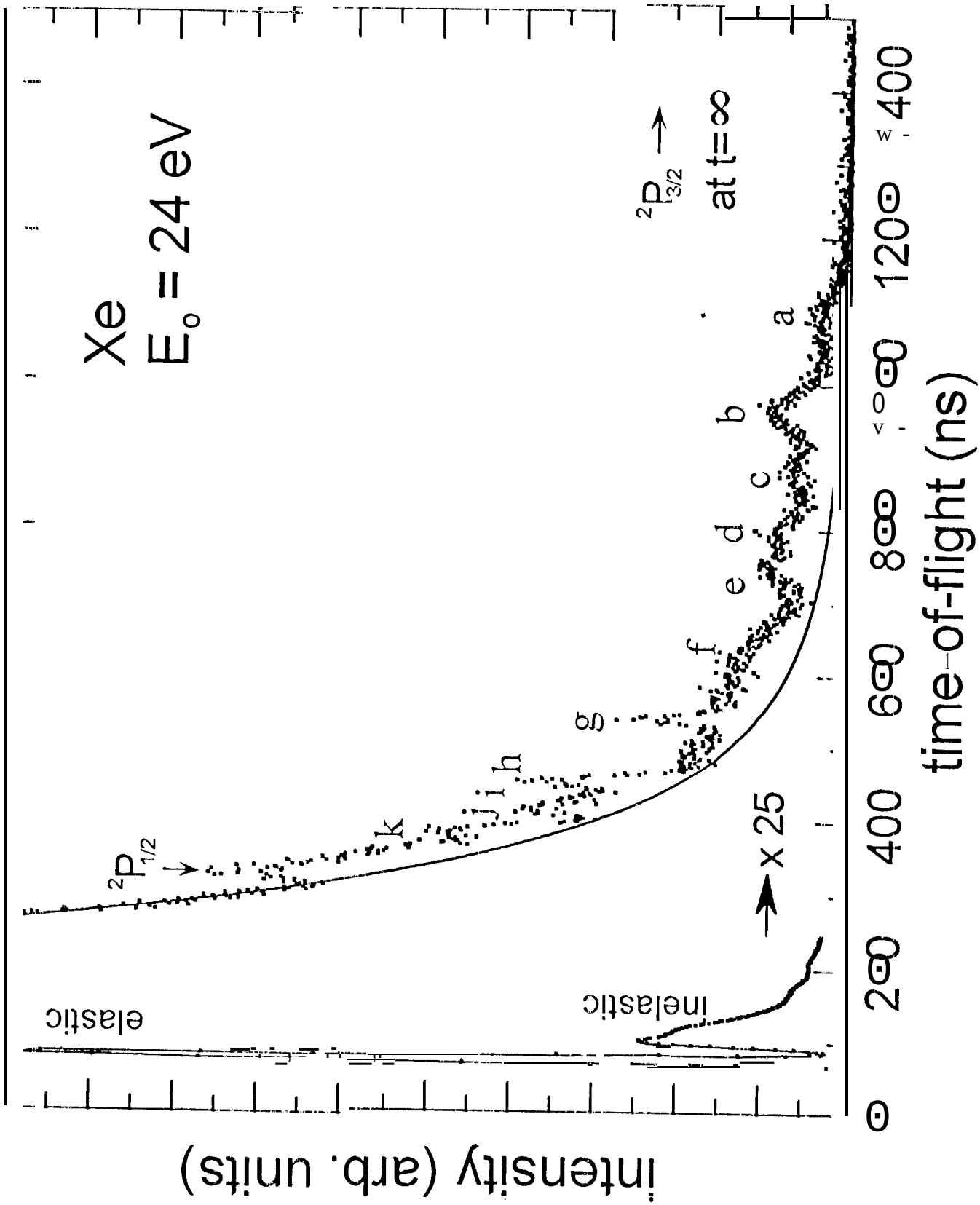
Xe
E° = 24 eV
$^2P_{3/2}$ → at t=∞
$^2P_{1/2}$ →
elastic
inelastic
× 25
a
b
c
d
e
f
g
h
i
j
k
intensity (arb. units)
time-of-flight (ns)
0
200
400
600
800
1000
1200
1400

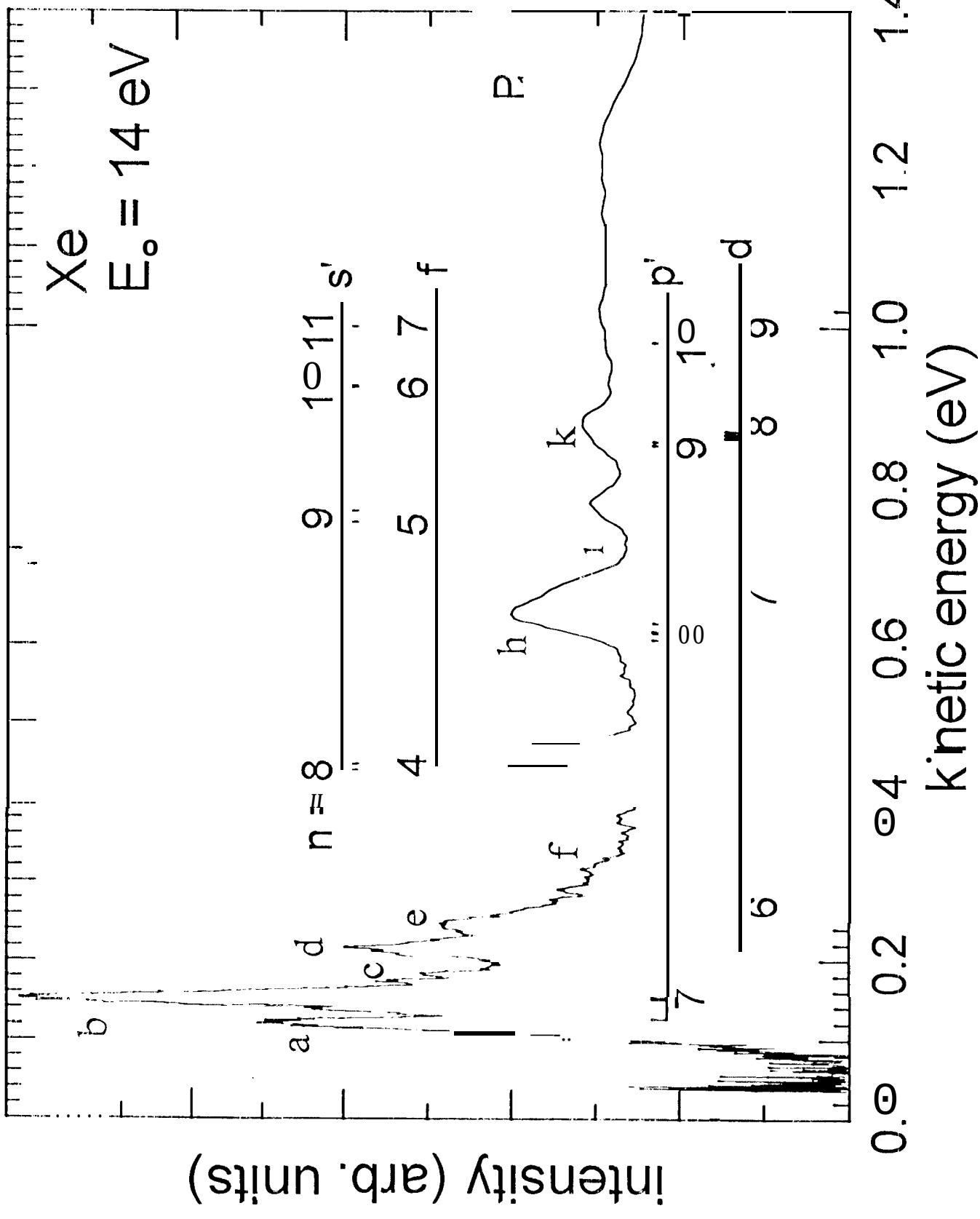
Xe
E° = 14 eV
n = 8
9
10
11
s'
4
5
6
7
f
p'
d
a
b
c
d
e
f
h
k
l
m
00
6'
7
8
9
10
0.0
0.2
0.4
0.6
0.8
1.0
1.2
1.4
kinetic energy (eV)
intensity (arb. units)

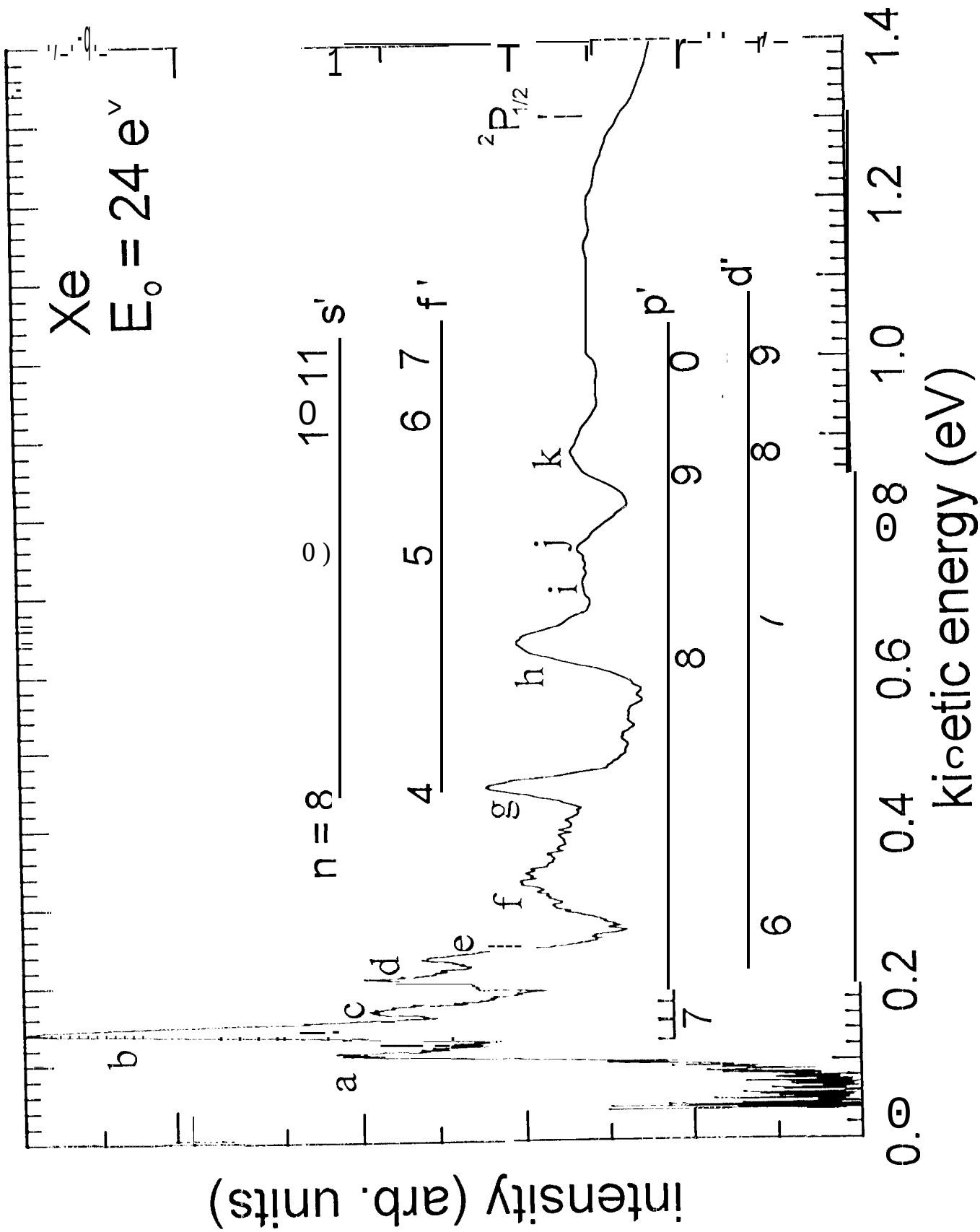
Xe
E₀ = 24 eV
intensity (arb. units)
kinetic energy (eV)
0.0
0.2
0.4
0.6
0.8
1.0
1.2
1.4
$^2P_{1/2}$
n = ∞
4
5
6
7
10
11
s'
f'
p'
d'
a
b
c
d
e
f
g
h
i
j
k

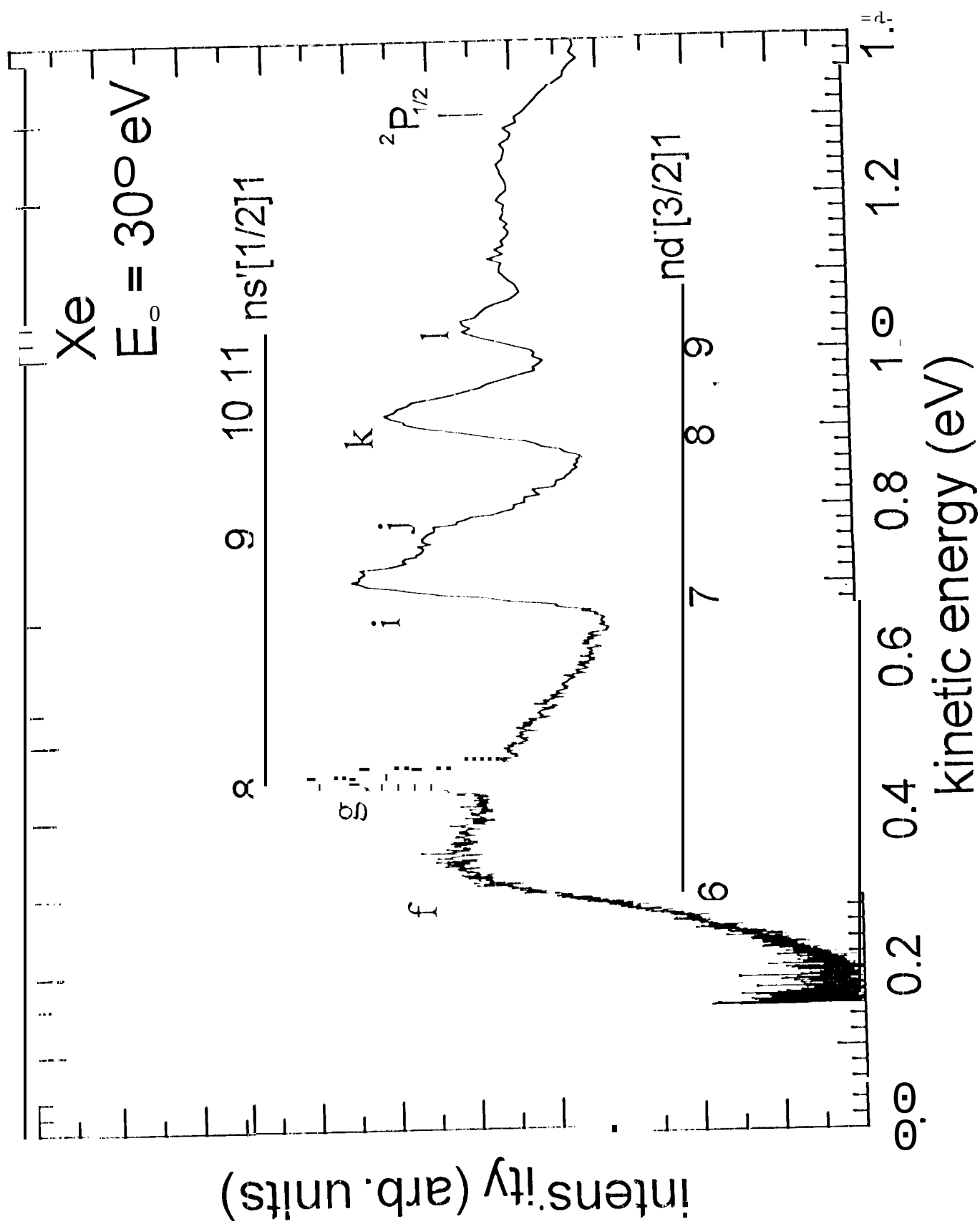
Xe
E0 = 30 eV
ns'[1/2]1
nd'[3/2]1
2P1/2
9
10
11
8
7
6
1
α
β
f
i
j
k
0.0
0.2
0.4
0.6
0.8
1.0
1.2
kinetic energy (eV)
intensity (arb. units)

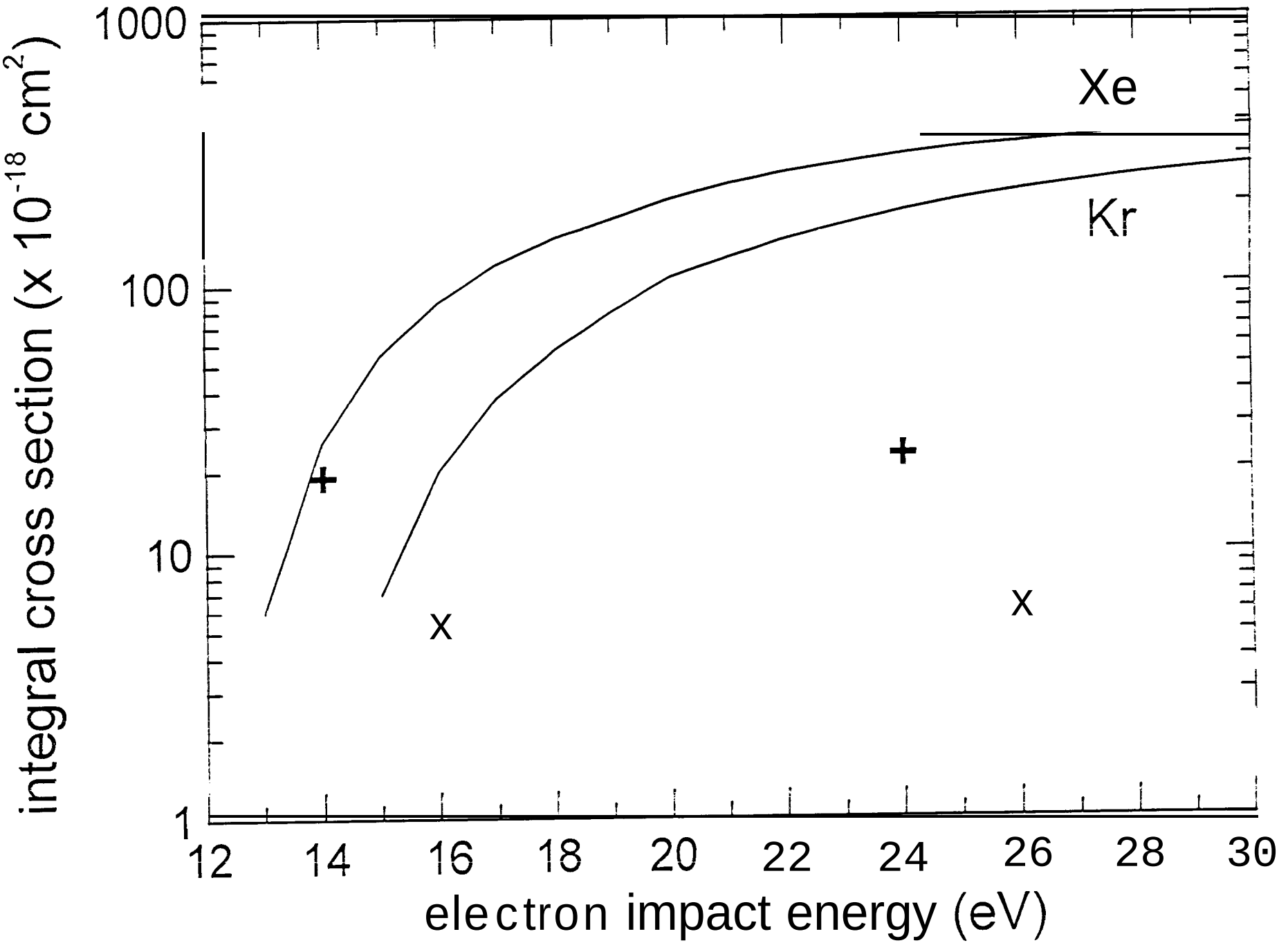

LeClair & Trajmar Fig. 5

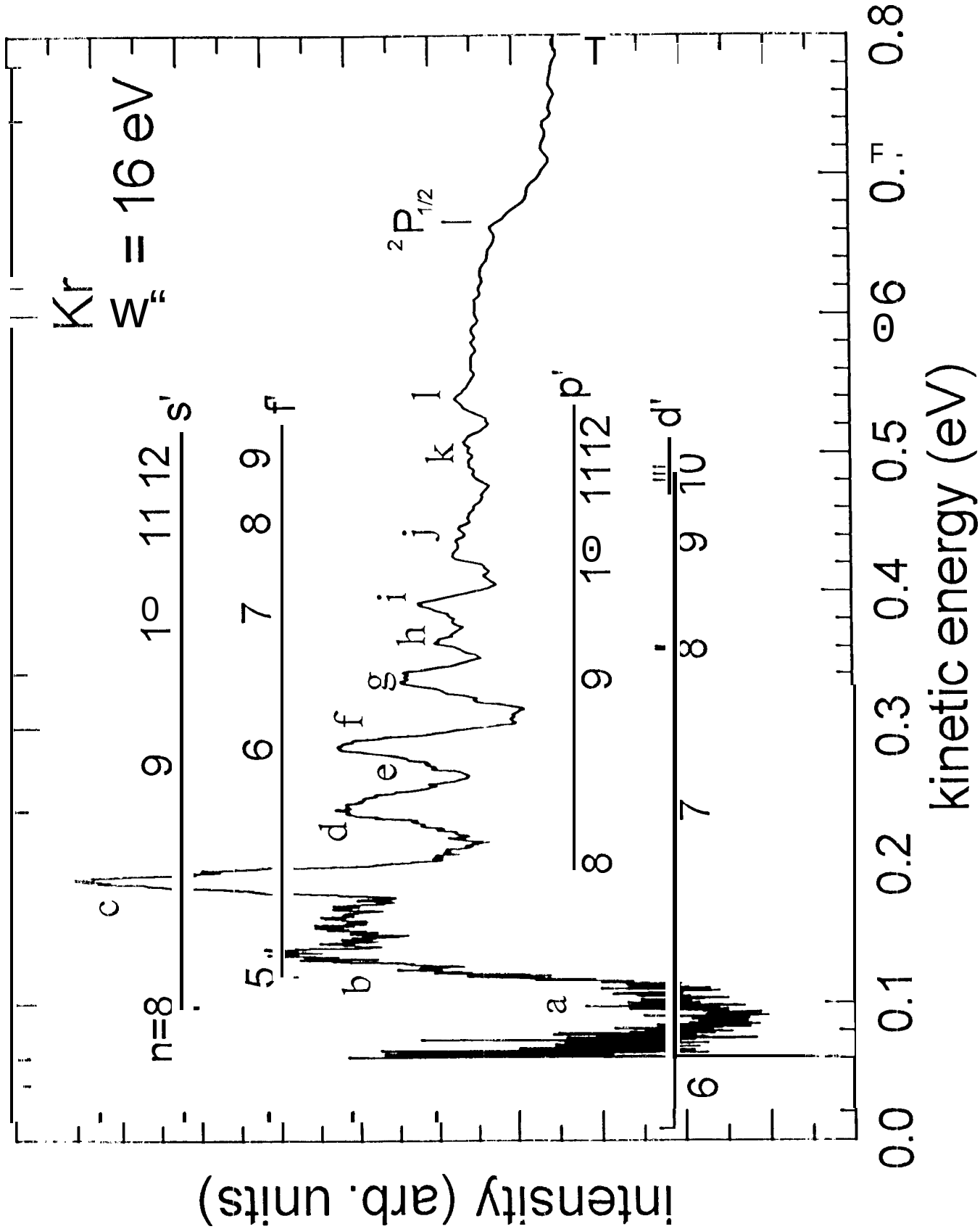
Kr
W"
= 16 eV
T
$^2P_{1/2}$
n=8
5"
s'
f'
p'
d'
a
b
c
d
e
f
g
h
i
j
k
l
0.0
0.1
0.2
0.3
0.4
0.5
0.6
0.7
0.8
kinetic energy (eV)
intensity (arb. units)

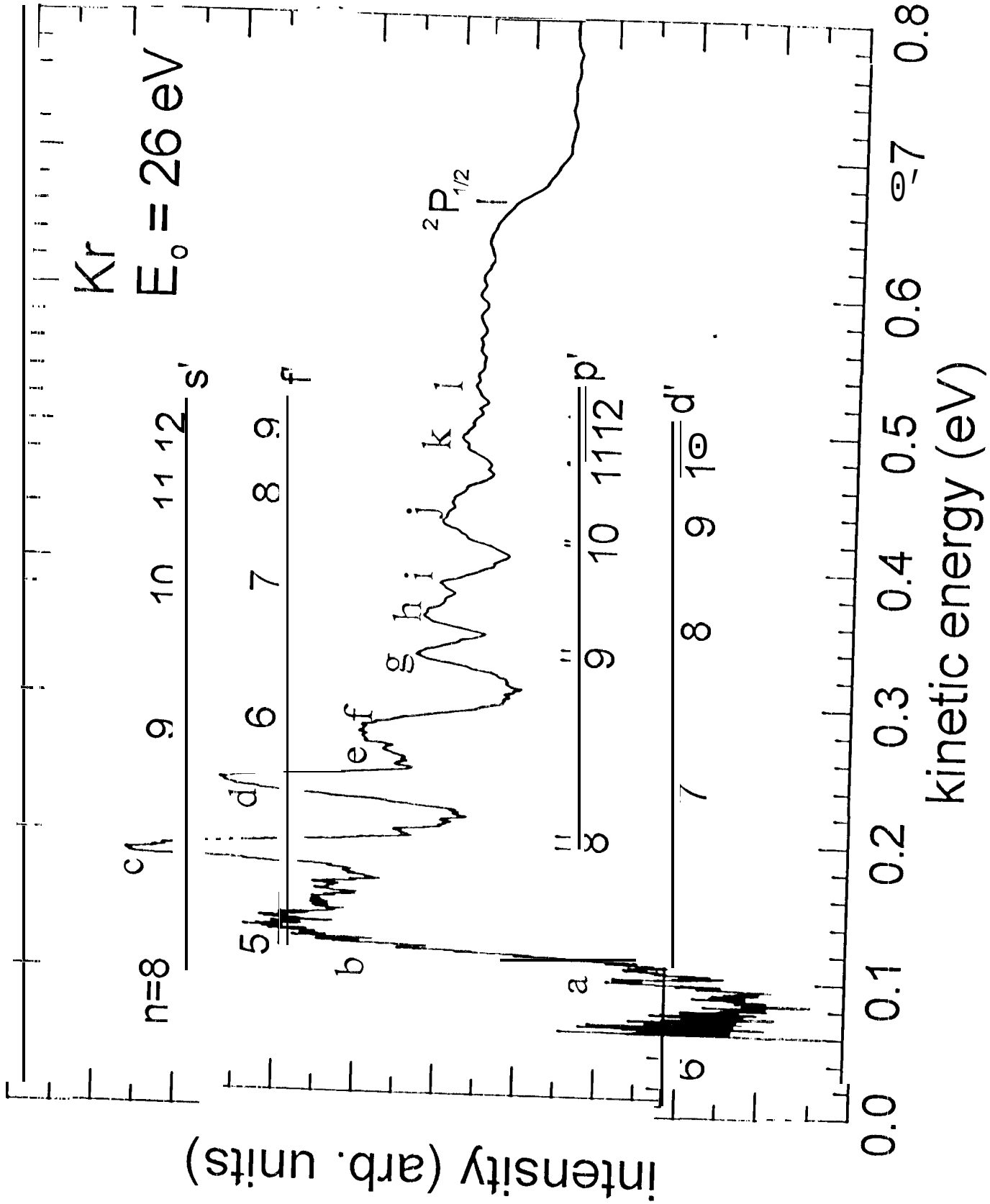
Kr
E_o = 26 eV
$^2P_{1/2}$
$^2P_{3/2}$
n=8
9
10
11
12
s'
5
6
7
8
9
f'
d'
p'
a
b
c
d
e
f
g
h
i
j
k
l
intensity (arb. units)
kinetic energy (eV)
0.0
0.1
0.2
0.3
0.4
0.5
0.6
0.7
0.8